JOURNAL OF CATALYSIS 107, 221–231 (1987)

Ammonia Synthesis over Supported Iron Catalyst Prepared from Amorphous Iron–Zirconium Precursor

I. Bulk Structural and Surface Chemical Changes of Precursor during Its Transition to the Active Catalyst

A. BAIKER,* R. SCHLÖGL,† E. ARMBRUSTER,‡ AND H. J. GÜNTHERODT‡

Department of Industrial and Engineering Chemistry, Swiss Federal Institut of Technology (ETH), ETH-Zentrum, CH-8092 Zürich, Switzerland; †Fritz-Haber Institut der Max Planck-Gesellschaft, 1000 Berlin 33, Federal Republic of Germany; and ‡Department of Physics, University of Basel, CH-4056 Basel, Switzerland

Received February 10, 1987; revised April 22, 1987

Active ammonia synthesis catalysts were prepared by *in situ* activation of amorphous $Fe_{91}Zr_9$ precursors in a continuous tubular fixed-bed reactor. When exposed to ammonia synthesis conditions (690 K, stoichiometric feed, 9 bar) the initially almost inactive amorphous $Fe_{91}Zr_9$ starts to crystallize and undergoes a sequence of structural and chemical changes which after about 500 hr on stream lead to a highly active and stable catalyst. This transformation occurs well below the bulk glass transition temperature of the amorphous precursor. The duration of the *in situ* activation can be reduced drastically by exposing the precursor to an oxygen pulse at reaction temperature. The activity of such catalysts is high compared to the activity of polycrystalline iron. The bulk structural changes which the precursor undergoes during its activation were investigated using X-ray diffraction, differential scanning calorimetry, and Mössbauer spectroscopy. The resulting stable active catalyst consists of iron particles which are stabilized by poorly crystalline nonstoichiometric ZrO_{2-x}. Two forms of iron can be distinguished: larger particles of well-crystalline α-iron, and as a minority phase, small particles of disordered iron with a considerably larger lattice constant. The latter phase is attributed to δ-iron. X-ray photoelectron spectroscopy revealed that the surface iron contains some oxide which may stabilize the active iron particles in a way similar to the way inclusion of iron aluminium oxide stabilizes the commercial ammonia synthesis catalyst.

INTRODUCTION

Metallic glasses possess several intrinsic properties which make them unique materials for catalytic studies. These attractive properties with respect to their application in catalysis are, among others, their large flexibility in the chemical composition as compared to that of equilibrium alloys, their high reactivity due to their metastable state, and their unique structure exhibiting only short-range ordering of the constituents. The potential of these materials to model supported metallic systems has been addressed recently (*1*).

Since their first application in catalysis (*2, 3*) reported in 1980, amorphous metals have gained growing interest as potential catalyst materials. Various amorphous metals have been found to exhibit excellent activity and/or selectivity in reactions such as hydrogenation and isomerization of olefins (*2, 4, 5*). CO hydrogenation (*3, 6, 7*), methanation (*8*), methanol synthesis (*9*), oxidation of methanol (*10*), and ammonia synthesis (*11*). A survey of these testing activities has been published very recently (*12*). The activation of the amorphous metal alloy was found to be a crucial step in virtually all investigations. Several activation procedures such as pretreatment in oxidizing or reducing gas atmosphere (*4–7, 10*), oxidation with nitric acid (*4*),

0021-9517/87 $3.00

reduction with zinc (*13*), and *in situ* reaction with the feed gas (*3, 8, 9, 11*) were applied to improve the catalytic properties of the amorphous metals. Comparatively little effort has been undertaken so far to characterize the chemical and structural changes which occur on the surface and in the bulk of these materials when they are exposed to pretreatment or reaction conditions.

We have reported recently in a preliminary communication (*11*) that a highly active ammonia synthesis catalyst could be obtained by *in situ* activation of an amorphous $Fe_{91}Zr_9$ alloy. The activity of as-prepared catalysts exceeds the activity of polycrystalline iron by more than an order of magnitude. The aim of the present work is to gain insight into the complex physical and chemical changes which occur in the bulk and surface of the amorphous precursor during its transition to the active catalyst.

In this paper, we report the changes of the bulk structure as studied by X-ray diffraction (XRD), differential scanning calorimetry (DSC), and Mössbauer spectroscopy, and the chemical changes of the surface investigated by photoelectron spectroscopy. In part 2 (*14*) of this series, we shall address the micromorphological changes of the surface during the genesis of the catalyst, using high-resolution scanning electron microscopy (SEM) and scanning tunneling microscopy (STM). Finally, in part 3 (*15*) we shall compare the nitrogen adsorption behavior and the ammonia synthesis kinetics over this catalyst with the corresponding behaviors known for more conventional systems, such as iron single crystals.

EXPERIMENTAL

Amorphous $Fe_{91}Zr_9$ was prepared as 0.5- to 1-cm-wide and about 30-μm-thick ribbons using the conventional melt spinning technique. Batches of ca. 20 g were obtained from premelted alloys in a high vacuum environment. The amorphous alloy was used either in the form of clippings (length 2–5 cm) or as flakes of 0.1–0.5 mm in size. The flakes were obtained by milling the ribbons in a centrifugal mill under liquid nitrogen which prevented both crystallization and oxidation. Both geometric forms of the alloy exhibited similar bulk and catalytic properties.

The ammonia synthesis activity tests were performed in a continuous flow tubular reactor using a stoichiometric feed of nitrogen and hydrogen (40 mL (STP)/min) at a total pressure of 9 bar. Detailed descriptions of the experimental setup and the feed gas purities have been reported elsewhere (*15*).

The BET surface areas of the precursor materials and the resulting active catalysts were determined using krypton adsorption at 77 K. Typical surface areas of the amorphous precursor materials were 0.02 m^2/g.

DSC experiments were performed on a Perkin–Elmer DSC 2B instrument in flowing nitrogen atmosphere. Heating rates were 10 or 20 K/min.

XRD experiments were carried out on a Siemens D 500 instrument with copper radiation. Flakes were analyzed on a rotating sample holder in conventional geometry. To avoid undesired background the ribbons were measured in transmission geometry. The *in situ* experiments were carried out in a modified Phillips APD 10 diffractometer system equipped with an Anton Parr hot stage and manual temperature controller. The gas flow of 3 : 1 H_2 and N_2 was mixed from research-grade pure gases and controlled with flow meters. A flux of ca. 40 mL/min through the volume of the camera of ca. 2 L was maintained. Qualitative chemical testing showed that ammonia was produced under experimental conditions.

Mössbauer spectra of ribbons and ground material were recorded after various catalytic experiments. A conventional transmission geometry with a 30 mCi Fe/Rh source was used at room temperature. The samples were loaded and kept under Ar

gas in a stainless-steel vacuum system equipped with beryllium windows.

Photoemission experiments were carried out in a Leybold LHS 10 electron spectrometer operating at 10^{-10} Torr base pressure. XPS and UPS data could be recorded from samples under various gaseous environments and temperatures between 80 and 900 K. Clean surfaces were obtained by Ar ion sputtering at 80 K. Ultraviolet photoelectron spectroscopy (UPS) data are presented without data treatment; the XPS results were adequately processed on a DS 5 computer system before presentation.

RESULTS

1. Activity and Bulk Structural Changes of Amorphous Alloy during in Situ Activation

Figure 1 shows the bulk structural properties of the amorphous $Fe_{91}Zr_9$ used in our study as seen by XRD and DSC. Both the XRD and the DSC characterizations indicate that the starting material was completely amorphous. The DSC curve shows that crystallization of the amorphous alloy sets in at about 840 K under the conditions used for the DSC measurement, i.e., under a nitrogen atmosphere and at a heating rate of 10 K/min.

Figure 2A depicts the change in ammonia synthesis activity of the amorphous precursor during *in situ* activation under ammonia synthesis conditions at 690 K and 9 bar total pressure. We note that the amorphous precursor is virtually inactive at the start of the *in situ* activation and that the activity

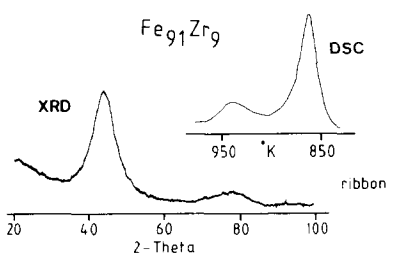

FIG. 1. Characterization of bulk structure of amorphous precursor by DSC and XRD. DSC was performed under a flowing nitrogen stream.

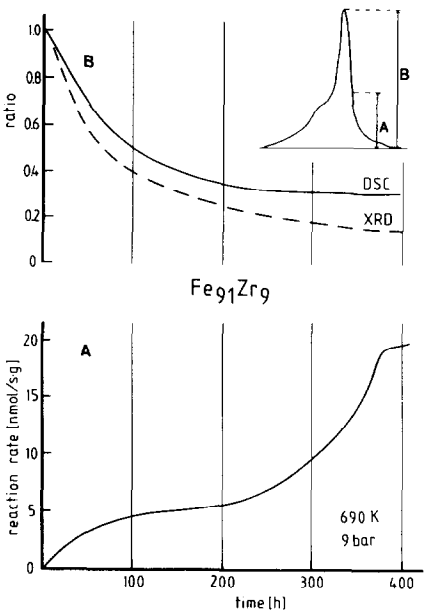

FIG. 2. (A) Change of activity of the amorphous alloy as a function of the time on stream during *in situ* activation under ammonia synthesis conditions (690 K, stoichiometric feed of 40 mL (STP)/min, 9 bar total pressure). (B) Crystallization of ribbons of an amorphous precursor with time on stream. DSC and XRD analyses were taken at nine points. The integral amount of heat evolved in the DSC of the residually amorphous material is plotted in the upper curve. The inset defines the ratio between well-crystallized α-iron and the additional phase which is plotted as dotted curve (see text).

increases steadily up to about 500 hr on stream, where the catalyst exhibits a stationary ammonia synthesis rate of about 20 nmol/g s. The shape of the activity curve was found to depend significantly on the amorphicity of the precursor material. Slight inhomogeneities in the structure of the amorphous materials resulted in marked changes in the shape of the activity curve. However, the general trend, i.e., the slow increase in the activity within 500 hr on stream, was observed with all samples investigated. Krypton adsorption measurements revealed that the BET surface area of the amorphous starting material (typically 0.02 m^2/g) increased significantly during the *in situ* activation. Increases in the surface area up to an order of magnitude were observed, depending on the activation

conditions and the homogeneity of the starting material.

A drastic reduction in the activation time down to a few hours was achieved when oxygen was admitted to the sample at reaction temperature. The oxygen pulse was obtained by replacing the hydrogen free reactant feed (nitrogen) by oxygen for 1–2 min. As a consequence of the oxygen pulse the catalyst bed temperature rose for a few minutes to ca. 800 K. The final activities of the fast (with oxygen pulse) and slowly activated catalyst (Fig. 2A) were similar. Both activation procedures led to catalysts with stable activity, as was evidenced by long-term tests over 2000 hr.

In order to gain further insight into the bulk structural changes of the precursor during the *in situ* activation we have performed a series of activation experiments in which the activation was stopped after various times and the catalyst was subjected to bulk structural characterization. The bulk structural changes of the precursor were investigated using XRD, DSC, and Mössbauer spectroscopy. The most obvious solid-state reaction occurring during the *in situ* activation was the crystallization of the amorphous starting material. Figure 2B shows the progress of crystallization of the amorphous precursor during the *in situ* activation (curve marked DSC). The relative amount of crystallization energy as measured by DSC is plotted as a function of the time on stream of the precursor. The alloy crystallized in part within the first 100 hr in parallel with the increase in activity. The second increase in activity between 250 and 380 hr is not reflected by a further loss of amorphous material. We note that after 400 hr on stream about 35% of the bulk catalyst still underwent an irreversible first-order phase transition. This behavior is interesting in the light that under inert gas atmosphere crystallization was observed at a higher temperature (840 K, DSC curve in Fig. 1) only. After 2000 hr on stream the catalysts have lost all their amorphous volume fraction.

Further insight into the bulk structural changes of the precursor occurring during its activation was gained by *in situ* high-temperature powder X-ray diffraction (XRD). Figure 3 shows wide scans from a ribbon of amorphous $Fe_{91}Zr_9$ in the high-temperature XRD. After a few hours at reaction temperature the broad pattern in the top trace was superimposed by the diffraction pattern of crystalline α-iron. The crystallization was complete after ca. 24 hr. It occurred only in the presence of hydrogen or the ammonia feed gas. Under vacuum (10^{-4} mbar) or inert gas, the amorphous diffraction pattern was preserved for several days at 700 K.

Closer analysis of the diffraction pattern of the crystallized sample reveals shoulders at the lower 2θ side of all iron peaks and a few weak broad reflections (e.g., around 30 and 48° 2θ) which arise from poorly crystallized zirconium oxide. The shoulders stay approximately constant in intensity, whereas the Bragg reflection for α-Fe (110) increases drastically with time. This apparent gradual reduction in the intensity ratio of the additional structure on the iron (110) line is shown in Fig. 2B (dashed curve in

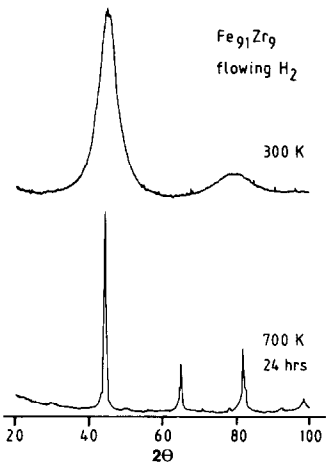

FIG. 3. *In situ* XRD of the transformation of the amorphous precursor (top trace) under flowing hydrogen into a three-phase mixture (bottom trace). The asymmetric footings of the principal α-iron reflections arise from the disordered iron minority phase.

the top plot). The inset gives the definition of the ratio A : B which was used to quantify the changes. The connection between crystallization and the evolution of the A : B ratio in XRD is given by the growth of the main peak for α-iron (increase in the absolute scattering power) as consequence of the crystallization.

We point out that this *in situ* XRD result is well reflected by the common observation of the lowering of the A : B ratio in the interrupted catalysis experiments which we reported previously.

Catalysts studied after 2000 hr on stream were completely crystallized as seen by DSC, but still showed in the XRD an A : B ratio of ca. 0.05. This, as well as the shape of the curves for the loss of the amorphous nature with time, indicates that the process of crystallization is nonlinear in time and seems to be kinetically still hindered at 700 K, much in contrast to crystallization experiments carried out at 900 K (*16, 17*).

Additional information was obtained from the various interrupted catalysis experiments with subsequent XRD analysis. Figure 4 summarizes the results for two analyses from catalysts taken at typical points in the activation curve (Fig. 2), namely, in the low activity region (top trace in Fig. 4) and in the final stage of activation (bottom trace in Fig. 4). We note the similarity of the general diffraction pattern with those obtained in the *in situ* XRD experiments. The patterns are considerably simpler than those obtained from samples crystallized under high vacuum at ca. 900 K. In these samples well-crystallized α-iron without the additional phase coexists with minority phases of Fe_2Zr and Fe_3Zr and well-crystallized zirconium oxide (beidelite). This crystallization pattern compares well with the second phase of crystallization described by Altounian *et al.* (*17*), except the formation of zirconia.

Comparison of the two wide scans in Fig. 4 shows the significant increase in scattering power for the activated sample, the iron (110) peak is nearly eightfold more intense

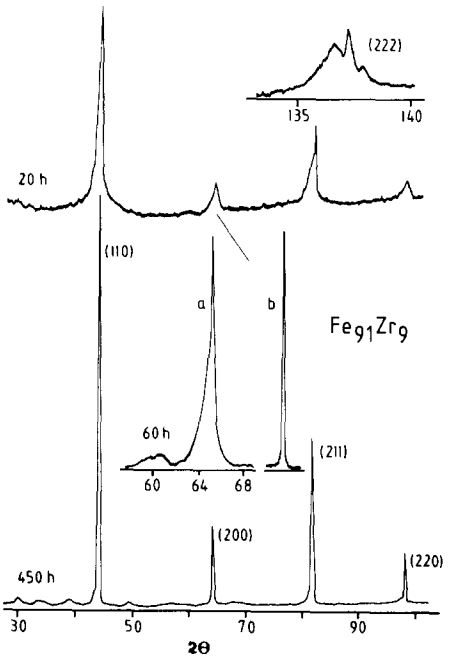

FIG. 4. XRD traces of catalysts derived from milled amorphous alloy after 20 hr (top) and 450 hr of activation under 9 bar of a 3 : 1 mixture of hydrogen and nitrogen at 700 K. The top inset shows a high-resolution scan over the Fe (222) reflection which consists of two doublets arising from the $CuK\alpha_1$/$CuK\alpha_2$ splitting. The central inset refers to the Fe (200) reflection which is shown after (a) 20 hr of activation and (b) from a thermally crystallized sample (see text).

than that in the top trace. The zirconium oxide phase is clearly visible in the bottom trace; it is however still poorly crystallized. The top trace demonstrates that the catalyst at this early stage of activation (Fig. 2) is largely crystallized; some remaining amorphous material broadens the footings of the (110) and the (211) peaks. The additional phase is clearly visible and high-resolution scans over the (200) and the (222) reflections demonstrate how the lines arising from well-crystallized α-iron are superimposed on a much broader reflection with a larger lattice constant. The inset for the (200) reflection compares this line (a) with the solely experimentally broadened reflection from iron obtained by thermal crystallization of $Fe_{91}Zr_9$ (b). In the lower trace the whole set of reflections from zir-

conium oxide is clearly visible. From the linewidth of these reflections a mean particle size of ca. 150 Å can be estimated. No reflections originating from Zr phases can be identified.

In order to further study the bulk structural changes associated with the activation process, we recorded room temperature Mössbauer spectra of several samples transferred under inert atmosphere from the microreactor. In Fig. 5 some typical spectra are displayed. The top spectrum originated from a fresh foil. It consists of an asymmetric doublet with a small isomer shift of −0.06 mm/s which has been interpreted as indicating a similar electronic structure of the alloy relative to pure iron. The electropositive Zr donates a small fraction of its valence electron density to iron which results in the negative sign of the isomer shift. Two individual lines with the same lineshape and the same width were fitted in all spectra of the amorphous alloy; different specimens showed a variable asymmetry of the two lines.

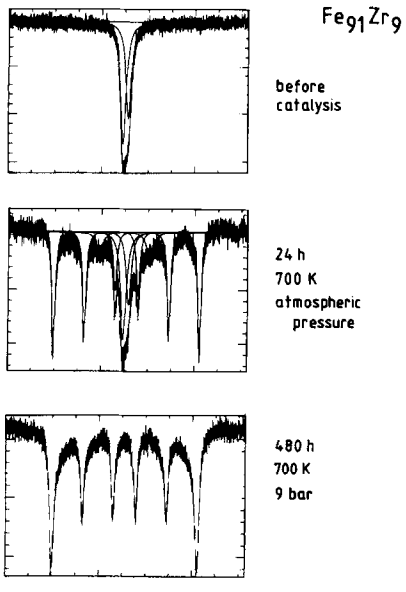

FIG. 5. Room temperature Mössbauer spectra of (a) the amorphous precursor, (b) the sample from the *in situ* XRD experiment (see Fig. 3), and (c) a milled activated catalyst. No significant deviations of the iron six-line pattern from the calibration spectrum of natural iron foil was found.

The central spectrum in Fig. 5 was taken from the sample used for the *in situ* XRD experiment (Fig. 3). Similar spectra were observed from samples after 60 and 150 hr of reaction, i.e., from samples in the early stage of activation (Fig. 2). The total spectrum consists of three subspectra which could be fitted and some minor contribution of ferric oxides which have not been taken into account. The most intense branches of these oxide spectra are visible in the corners of Fig. 5 central. The main spectra arise from the partly still amorphous alloy (central narrow doublet). A broad weak doublet with an isomer shift of −0.14 mm/s next to the central feature may arise from a Zr-rich Fe–Zr alloy. Clearly visible is the typical six-line pattern of α-iron indicating with its intensity distribution a random orientation of the iron crystals.

The bottom spectrum in Fig. 5 is typical for fully activated (480 hr on stream) catalysts. Attempts to fit the spectrum with two sets of six-line patterns were unsuccessful and thus no fit is presented in this case. The predominant six-line pattern arises, however, from metallic iron. The intensity distribution is indicative of preferred orientation of at least part of the iron crystals relative to the gamma ray beam. Note that at this stage of a fully activated catalyst no trace of amorphous alloy is present, not even in the bulk of the sample.

2. *Chemical Structure of Catalyst Surface*

The chemical structure of the catalyst surface was investigated using X-ray photoelectron spectroscopy (XPS) and ultraviolet photoelectron spectroscopy. We present only results from experiments in which the catalysts have been transferred from the reactor immediately into the UHV under strict retention of a protective gas atmosphere. However, superficial oxidation of reactive iron could not be excluded completely.

First we investigated the valence structure of the fresh catalyst at 700 K reaction temperature. Traces 1 and 2 in Fig. 6 represent the electronic structure of the surface as seen by the feed gas in the initial moment of activation. The sample from trace 1 was thermally crystallized in the UHV and had lost the metallic character of the top surface (no Fermi edge detectable). The amorphous sample (trace 2) shows a residual metallic character from the peak containing the Fermi edge. It arises most likely from iron 3*d* states. The intense structures beyond 5 eV are due to oxides being the most abundant surface species in both samples.

An amorphous precursor transferred after 1000 hr on stream (700 K, 9 bar, various N_2-to-H_2 ratios) gave the top spectrum in Fig. 6. There is no indication of a metallic character at all; the sample is completely covered with an insulating oxide film. This film is, however, still thin enough to prevent charging of the sample. Note that this result does not indicate that the working catalyst surface is of an oxidic nature. The thin oxide layer points to a high sensitivity of the active catalyst against traces of oxygen which cannot be avoided during the transfer.

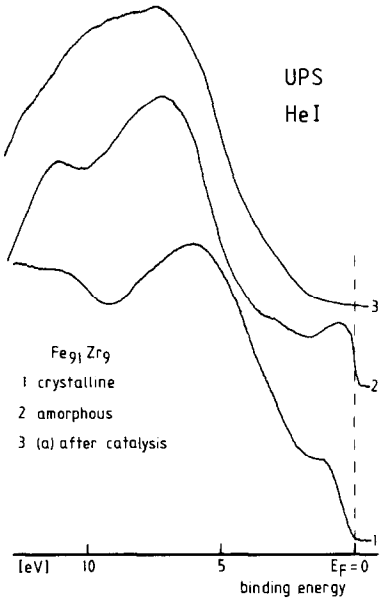

FIG. 6. Helium (I) UPS spectra of various alloy surfaces at 700 K in UHV. The Fermi level is calibrated against a Pd foil. The crystalline sample was obtained from the amorphous one by *in situ* heating to 900 K for 4 hr.

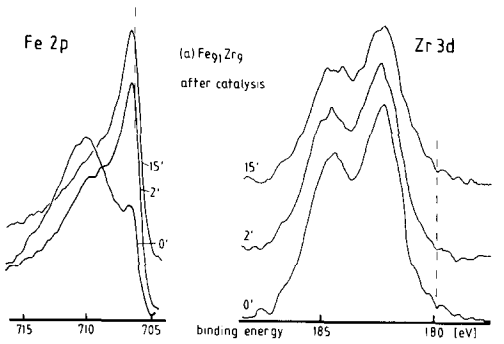

FIG. 7. XPS core level spectra of fully activated ribbons. Times in minutes refer to Ar sputtering (scanning ion source at 5 kV with 10 mA emission at 2 × 10^{-6} Torr). The dotted lines denote centroid positions of elemental Fe (2*p*-3/2) and Zr (3d-5/2).

Another task of the XPS investigation was the evaluation of the elemental composition of the chemical structure of the activated catalyst surface. In order to explore the artificial oxidation we used gentle argon ion etching to examine the surface near the original catalyst surface and by more severe etching information related more closely to the bulk of the catalyst could be obtained. In Figs. 7 and 8 we present typical results from a catalyst which had been used for 360 hr at 720 K and 9 bar of

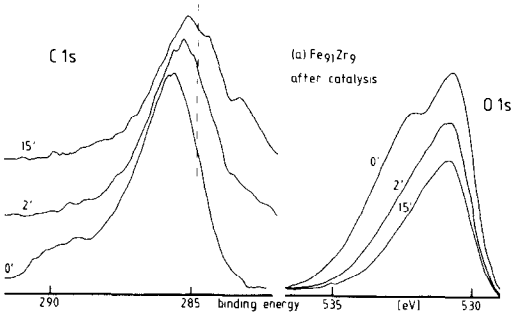

FIG. 8. XPS core level spectra of major impurities in the surface of fully activated ribbons. Times in minutes refer to the sputter cleaning (see Fig. 7 and text).

stoichiometric feed. The ion dose quoted in the figures yielded an equivalent sputtering of ca. 20 Å for 2 min and 300 Å for 15 min with a smooth gold film.

Figure 7 presents the core level spectra of the nominal constituents of the catalyst. The outer surface is covered with iron oxide (in hematite-like forms) and zirconium oxide (nonstoichiometric ZrO_{2-x}). In the iron 2*p* spectrum a contribution of metallic iron is visible indicating that the surface oxide film is thin within the information depth of XPS (ca. 25 Å), but homogeneous as follows from the absence of a Fermi edge in the more surface-sensitive UPS (Fig. 6, trace 3). Gentle sputtering removed most of this film and left some ferrous oxide besides the predominant metallic iron. Significantly, there is little change in the zirconium spectrum and even after prolonged sputtering there is no metallic zirconium to be detected (for positions of the main elemental peaks see dotted reference lines in Fig. 7).

Even after sputtering for 2 hr the iron could not be obtained in pure metallic form. Some intensity persisted around 710 eV which cannot be attributed to the many-body satellite spectrum of the metal. It is indicative of ferrous oxide. This observation is in line with the traces of oxide found in the Mössbauer spectra.

In Fig. 8 spectra from the main impurity elements carbon and oxygen are displayed. We conclude from comparison with spectra of the unused catalyst that the carbon content of the used catalyst originated from impurities of the feed gas. The precursor material only contained the usual surface carbon species which was completely removed after 2 min sputtering. The main contribution to the intensity in the C 1*s* spectra arises from a carbonaceous deposit probably formed by coking of hydrocarbons synthesized from the feed impurity. The dotted line gives the centroid position of the C 1*s* emission of bulk carbon black. The structure at 289 eV in the top surface spectrum points to the presence of carbonyl groups at the surface of the deposit. The shoulder at the low binding energy side of the 15-min sputtered sample indicated the presence of a carbide form in the subsurface region of the catalyst. We found that the carbon could not be removed completely by sputtering for 2 hr.

The oxygen 1*s* signal from the top surface is clearly split into two components. At 531 eV, we observe oxygen from oxides of zirconium and iron. The peak at 532 eV arises from chemisorbed water and hydroxyl groups present on the metal oxides. Sputtering reduces the intensity of the oxygen spectrum significantly, but oxides as well as hydroxyls remain on the predominantly metallic surface. This implies a microstructure in which bulk oxide particles coexist with largely metallic areas.

Table 1 lists some typical chemical compositions of the surface region of the precursor and of the active catalyst. A comparison of the chemical compositions of the amorphous precursor and the active catalyst indicates that as a result of the *in situ* activation both the oxygen and the carbon contents of the sample increased markedly. The sputtering experiments indicate that both increases originate mainly from feed gas impurities (O_2, CO). We note that besides the main components (iron, zirconium, oxygen, and carbon) minor impurities of silicon, copper, and nitrogen were detected. Copper was incorporated into the alloy during the rapid solidification process on the copper wheel. It is only present in the contact surface of the ribbons; the free surface is free of copper. Silicon was incorporated into the top surface of the catalyst in the reactor bed which contained quartz sand and a quartz fritt. Both contaminants were completely removed after 15 min sputtering. Persistent however was the nitrogen impurity which resulted in a small but discernible peak at 397 eV. This is ascribed to the presence of a small amount (between 1 and 5 at.%) of zirconium nitride at the surface and in the subsurface region of the catalyst.

TABLE 1

Elemental Composition of Surface Region of Catalyst Obtained from Amorphous $Fe_{91}Zr_9$ Precursor as Determined by XPS[a]

Sample		Concentrations[b]				
		% Fe	% Zr	% O	% C	Others
(A) Fresh precursor before use	Top surface	14.1	2.9	63.4	19.2	traces Cu, N
	Ar sputtering 5 min	77.7	8.6	10.5	3.1	
(B) After 210 hr on stream, transferred in argon		48.9	14.8	23.4	12.8	
(C) After 500 hr on stream, transferred in air	Top surface	20.5	4.2	54.3	18.0	2% Si, 0.8% N, S
	Ar sputtering 2 min	44.7	3.7	37.2	14.5	
	15 min	54.2	3.4	32.3	11.3	
(D) Precursor crystallized		11.0	39.3	37.2	12.4	

[a] Sputtering conditions: 2×10^{-6} Torr, 10 mA emission, 5.0 kV with 25 mm distance source to sample.

[b] Integrals calculated using Scofield cross sections of Fe 2*p*, Zr 3*d*, O 1*s*, C 1*s*, N 1*s*, and Si 2*p*.

DISCUSSION

1. Activity and Bulk Structural Changes of Amorphous Alloy during in Situ Activation

The inactivity of the amorphous $Fe_{91}Zr_9$ precursor at the beginning of the *in situ* activation (Fig. 2A) is attributed to the thin oxide layer covering its surface. After reduction of this superficial oxide layer the activity starts to develop but still remains relatively low. An *in situ* activation of about 500 hr is necessary to reach stationary activity. This maximum activity has been shown to exceed the activity of similarly pretreated polycrystalline iron by more than an order of magnitude (*11*).

The most obvious changes in the bulk structure of the amorphous precursor during activation are the crystallization and the transformation of zirconium to zirconium oxide. The importance of the zirconia formation, i.e., of the role of oxygen, is supported by the fact that the activation time could be reduced drastically if the precursor was subjected to an oxygen pulse during the *in situ* activation. The crystallization has been shown to be closely related to the activation of the catalyst (Fig. 2B). It is of paramount importance in the understanding of the catalytic activity of the amorphous alloy which is in its as-cast state almost inactive. The access to a metastable form of iron in the surface near regions may well be the structural answer to the question of the active principle in these materials. According to our observations and to literature studies (*16, 17*), crystallization of an iron–zirconium alloy is not a simple process involving a single first-order phase transition; rather, it comprises a sequence of events, the order and duration of which depend crucially on the experimental conditions. The whole process is not isotropic but may occur at the surface or certain other activated sites first and later in the bulk. This view is further supported by the micromorphological observations described in part 2 (*14*).

Our XRD investigations show that crystallization of the amorphous precursor under ammonia synthesis conditions leads

predominantly to well-crystallized α-iron with the usual lattice constant of 2.86 Å, and a small fraction of a minority phase with a considerably larger lattice constant and with much less crystalline perfection. The zirconium part is transformed in poorly crystallized zirconia. The minority phase may be ascribed to δ-iron. Its lattice constant of 2.905 Å (*16*) agrees well with our observations.

The crystallization of the amorphous precursor occurring during *in situ* activation under ammonia synthesis conditions was found to be completely different from thermally induced structural relaxation. Our comparative crystallization studies by means of XRD indicate that the crystallization temperature is reduced drastically under ammonia synthesis conditions or under a hydrogen atmosphere. Furthermore, the crystallizations led to different bulk structures of the crystalline materials, depending on the ambient gas phase. Under inert gas atmosphere or under vacuum our results agree with the bulk observations described by Altounian *et al.* (*17*). Finally, we should emphasize that all our bulk structural investigations indicate that there is no alloy present in the activated catalyst.

2. *Chemical Structure of Catalyst Surface*

The concentrations of the nominal constituents (Table 1) are discussed by the Fe-to-Zr ratio rather than by their absolute values due to the high level of "impurities" in the samples. The nominal ratio for the precursor alloy is 10.11. All top surfaces are strongly enriched in Zr and O which is attributed to chemically induced segregation by formation of zirconia. Consequently, Zr is depleted in the inner regions of the material as seen with the fully activated catalyst. Extensive sputtering of the unused catalyst (precursor) resulted in the expected ratio of 10.1. Thus the observed deviations are due to chemically induced segregation and oxidation and are not typical for the bulk of the catalyst material. This is illustrated by the extensive Zr segregation upon thermal crystallization in a UHV environment (Table 1). The enrichment of Zr exceeds the segregation in the amorphous precursor and in the catalysts during all stages of activation by far and thus indicates for the surface that thermal crystallization is a different phenomenon from the crystallization associated with activation of the catalyst.

In general we note the high concentration of carbon in all catalysts. Most of the carbon exists in the form of a carbonaceous deposit which was probably formed by coking of hydrocarbons synthesized from impurities of CO contained in the feed.

Regarding the absolute surface concentration of iron we find the intermediately activated and immediately transferred catalyst to contain ca. 50% iron. A similar content is found for the shortly sputter-cleaned fully activated sample. Note that this is a considerably higher concentration than the one usually found for multiply promoted industrial catalysts which was quoted to be less than 10% (*18*). However, this value may critically depend on the reduction conditions applied.

The surface iron seems to contain some oxide which may stabilize the catalyst in a way similar to the way inclusion of iron aluminium oxide stabilizes the commercial ammonia synthesis catalyst. In the present case the iron oxide or iron zirconium oxide may act as a structural promoter by forming a mixed oxide–metal surface. This interpretation of the XPS sputtering results is in line with the observation of the disordered iron species in the XRD experiments.

Finally we note that the catalysts used showed very little nitridation of their surfaces. This is ascribed to the low conversion maintained in the test runs which kept the hydrogen partial pressure high with respect to the ammonia partial pressure.

CONCLUSIONS

Amorphous $Fe_{91}Zr_9$ was found to be an excellent precursor for the preparation of ammonia synthesis catalysts. When ex-

posed to ammonia synthesis conditions the amorphous alloy crystallizes slowly and concomitantly structural and chemical changes in the bulk and at the surface occur which finally lead to a highly active catalyst. The observation that the activity increases upon crystallization, i.e., with growing iron particle size, is fully in line with the structure sensitivity found for ammonia synthesis over supported iron (*19*). The slow activation can be accelerated drastically by exposing the precursor to a short pulse of oxygen during the *in situ* activation. The active catalyst consists of iron particles which are stabilized by poorly crystallized zirconia. The catalytically active species is iron, which exists in two predominant forms: well-crystallized α-iron with the usual lattice constant, and a small fraction of iron with a considerably larger lattice constant and much less crystalline perfection. The minority phase has a lattice constant which agrees well with the one reported in the literature for δ-iron. The content of iron on the surface of the active catalyst was found to be about 50%.

ACKNOWLEDGMENTS

Thanks are due to P. Reimann for preparing the samples used. One of us (R.S.) is grateful to the Swiss National Science Foundation for financially supporting his stay at Basel. The whole project was financially supported by LONZA AG, Switzerland.

REFERENCES

1. Yoon, C., and Cocke, D. L., *J. Non-Cryst. Solids* **79,** 217 (1986).
2. Smith, G. V., Brower, W. E., Jr., Matyjaszczyk, M. S., and Pettit, T. L., *in* "Proceedings, 7th International Congress on Catalysis" (Seiyama, T., and Tanabe, K., Eds.), p. 355. Elsevier, New York, 1981.
3. Komiyama, H., Yokoyama, A., Inoue, H., Masumoto, T., and Kimura, H., *Sci. Rep. Res. Inst. Tohoku Univ. Ser. A* **28,** 217 (1980); Yokoyama, A., Komiyama, H., Inoue, H., Masumoto, T., and Kimura, H., *Catalysis* **68,** 355 (1981).
4. Yoshida, S., Yamashita, H., Funabiki, T., and Yonezawa, T., *J. Chem. Soc. Faraday Trans. 1* **80,** 1435 (1984).
5. Baiker, A., Baris, H., and Güntherodt, H. J., *J. Chem. Soc. Chem. Commun.* 930 (1986).
6. Kisfaludi, G., Lazar, K., Schay, Z., Guczi, L., Fetzer, C., Konczos, G., and Lovas, A., *Appl. Surf. Sci.* **24,** 225 (1985).
7. Peuckert, M., and Baiker, A., *J. Chem. Soc. Faraday Trans. 1* **81,** 2797 (1985).
8. Yokoyama, A., Komiyama, H., Inoue, H., Masumoto, T., and Kimura, H., *J. Non-Cryst. Solids* **61,** 619 (1984).
9. Shibata, M., Ohbayashi, Y., Kawata, N., Masumoto, T., and Aoki, K., *J. Catal.* **96,** 296 (1985).
10. Kawashima, A., and Hashimoto, K., "Proc. 4th Int. Conf. Rapidly Quenched Metals" (Masumoto, T., and Suzuki, K., Eds.), Vol. II, p. 1427. 1982.
11. Armbruster, E., Baiker, A., Baris, H., Güntherodt, H. J., and Schlögl, R., *J. Chem. Soc. Chem. Commun.* 299 (1986).
12. Shibata, M., and Masumoto, T., *in* "Preparation of Catalysts IV" (Grange, P., Jacobs, P. A., and Poncelet, G., Eds.), p. 353. Elsevier, Amsterdam, 1987.
13. Hashimoto, K., Kawashima, A., and Sakai, K., Japanese Patent 200565, 1982.
14. Schlögl, R., Wiesendanger, R., and Baiker, A., submitted for publication.
15. Baiker, A., Baris, H., Schlögl, R., submitted for publication.
16. Fujinami, M., and Ujihira, Y., *J. Appl. Phys.* **59,** 2387 (1986).
17. Altounian, Z., Batalla, E., and Strom-Olsen, J. O., *J. Appl. Phys.* **59,** 2364 (1986).
18. Silverman, D. C., and Boudart, M., *J. Catal.* **77,** 208 (1982).
19. Boudart, M., Topsoe, H., and Dumesic, J. A., *in* "The Physical Basis for Heterogeneous Catalysis" (E. Drauglis and R. I. Jaffe, Eds.), p. 337. Plenum, New York, 175.